Journal of Constructional Steel Research 67 (2011) 690–705

Contents lists available at ScienceDirect

Journal of Constructional Steel Research

journal homepage: www.elsevier.com/locate/jcsr

Cyclic behavior of bolted connections with different arrangement of bolts

Mohsen Gerami [a], Hamid Saberi [a,*], Vahid Saberi [a], Amir Saedi Daryan [b]

[a] Department of Civil Engineering, University of Semnan, Semnan, Iran

[b] Member of Young Researchers Club (Islamic Azad University, North Branch), Iran

ARTICLE INFO

Article history:
Received 21 April 2010
Accepted 16 November 2010

Keywords:
Cyclic behavior
Bolted connections
End plate
T-stub
Failure mode
Bolt arrangement

ABSTRACT

During the 1994 Northridge earthquake, relatively poor performance of the bolted web-welded flange connections (BWWFs) was observed. Thereafter, various types of connections such as end plate and T-stub bolted connections were suggested to be used in moment resisting frames that are often used in industrial and tall buildings. In this paper, finite element simulation is used to study and compare the cyclic behavior of fourteen specimens of the mentioned connection type by changing the horizontal and vertical arrangement of bolts. The results show that the moment capacity and the initial rotational stiffness of T-stub bolted connections are higher than that of end plate bolted connections designed based on AISC considering the total energy dissipation of both groups to be approximately equal. It is also evident that the probability of failure mode change in T-stub connections is higher than that of end plate connections under cyclic loading due to the arrangement variation of bolts. Based on the results of this paper, end plate connections are suggested for conditions where the imperfection in construction is probable.

1. Introduction

Moment resisting frames are widely used in areas of high seismic activity. They exhibit high redundancy and high energy dissipating capabilities. In contemporary seismic-resistant design, it is common to design moment resisting frames to develop plastic hinges in the beams while preventing hinges to be developed in the columns, since it tends to improve the lateral stability of the structure. The integrity of moment resisting frames lies largely on the ability of the connections to transmit moments and shear between the beams and columns [1].

Among some of the most commonly used moment connections, the bolted web-welded flange connection (BWWF) was believed to provide the necessary attributes to ensure the required performance under seismic loading. During the 1994 Northridge and the 1995 Hyogo-Ken Nanbu earthquakes, however, relatively poor performance of the BWWF connection was observed [2–6]. The welds, predominately the bottom flange welds, in some of the BWWF connections suffered from severe cracking. Following the discovery of these failures, numerous experimental and analytical investigations were initiated to obtain a moment connection that will provide the required combination of strength, stiffness, and ductility while resisting cracking. Therefore, various types of connections such as end plate and T-stub bolted connections were suggested to be used in design of moment resisting frames in areas of high seismic activity. Since bolted connections include more details such as bolts, angles, T-stubs and plates that cause congestion at connection zone, the inelastic behavior of such connections is intrinsically more complicated than welded connections. High energy dissipating capabilities and suitable ductility will be observed if such connections are designed properly. Since the welding of these connections is performed in the shop under controlled conditions and in the most favorable position, high quality welds are easier to be achieved with this type of connection compared with field-welded connections.

In recent years, several research have been conducted to investigate the beam-to-column bolted connections. Some of these studies are as follows:

A series of tests on the four-bolt extended unstiffened and the eight-bolt extended stiffened moment end plate connections and a validation study utilizing the finite element method were conducted as a part of the SAC Steel Project. It was determined that the extended moment end plate connections can be designed to provide a great deal of ductility in seismic force resisting moment frames and that the finite element method can be used to predict the behavior of end plate connections [7].

The experimental analysis of two specimens of bolted T-stub connections under cyclic loads was investigated. Specimen 1 had rectangular-shaped stems, whereas Specimen 2 had U-shaped stems and location of bolts on its stem was slightly closer to the

* Corresponding author. Tel.: +98 2122099187; fax: +98 2122751397.
E-mail addresses: mgerami@semnan.ac.ir (M. Gerami), saberi.hamid@gmail.com (H. Saberi), saberi.vahid@gmail.com (V. Saberi), amir_saedi_d@yahoo.com (A. Saedi Daryan).

0143-974X/$ – see front matter © 2010 Elsevier Ltd. All rights reserved.
doi:10.1016/j.jcsr.2010.11.011

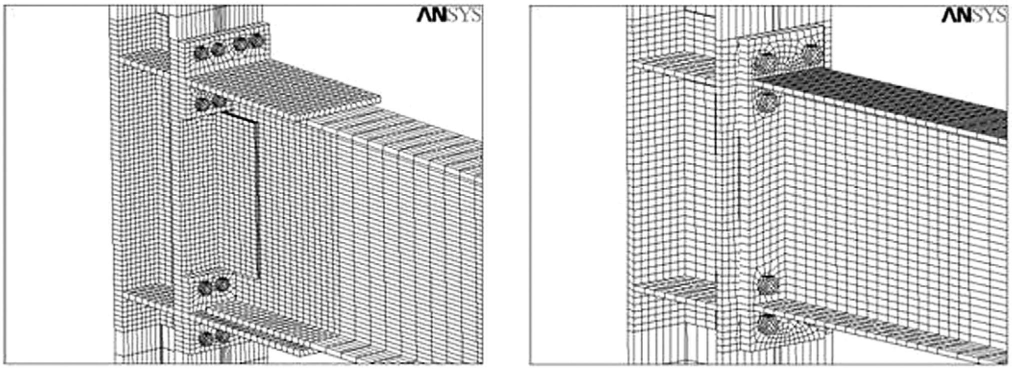

(a) Finite element mesh "Specimen 1". (b) Finite element mesh "4E-1.5-1.25-24".

Fig. 1. Schematic view of the specimens used for validation of numerical and experimental results.

end of the fillet weld. The test of Specimen 2 demonstrated that the use of 1 in. (25.4 mm) bolts in stems requires a greater distance between the bolt and the end of the fillet weld. Besides, their nonlinear analysis showed that the bolts used to connect the T-stub stem and the beam flange can be moved further from the column face (the set close to the face of the column) or even can be omitted completely [8,9].

The behavior of bolted T-stub connections made up of welded plates was investigated experimentally. The research was mainly concentrated on rolled profiles as T-stub elements. The results showed that the welding procedure is particularly important to ensure a ductile behavior of the connection [10].

An experimental investigation of eight statically loaded extended end plate moment connections was undertaken. The investigated parameters were the end plate thickness and steel grade. The results show that an increase in end plate thickness results in an increase in the connection flexural strength and stiffness and a decrease in rotation capacity. Similar conclusions are drawn for the effect of the end plate steel grade, though no major variations in the initial stiffness are observed [11].

Influence of initial imperfection (C, V, W shapes) on the behavior of extended bolted end plate connections for portal frames was investigated. The test results showed that initial rotation stiffness of extended bolted end plate joints decreases with increase of initial imperfection in the end plate, however, the strength of the end plate joints is slightly affected by the imperfection. Besides, the thicker the end plate is, the more reduction in the initial rotation stiffness relatively. The analytical results showed that among the three types of initial imperfection, the V-shape has the least influence, and the C-shape has the highest influence on the initial rotation stiffness of the extended bolted end plate joints [12].

The experimental behavior of blind bolted angle connections between open beams and tubular columns was done. Based on the findings, simplified approaches through which the initial stiffness and yield parameters can be estimated are assessed [13].

2. Scope of the study

The variations of design parameters in bolted connections, such as bolt arrangement variation, affect the cyclic behavior of these connections. These parameter variations could be due to the imperfections in construction. Thus, more accurate perception of behavioral influencing of such connections due to variation of the mentioned parameter will help the designers to choose appropriate connection according to the construction conditions. In the current study, to evaluate the accuracy of the finite element modeling approach, two finite element models are developed according to the corresponding experimental specimens and the results are compared with test results. After verification of FE models, two reference connections are designed based on AISC and then four finite element models with different bolt horizontal distance from centerline of beam web as well as six finite element models with different bolt vertical distance from beam flange are considered and the numerical results such as moment capacity, initial rotational stiffness, relative displacement between column flange and T-section flange or end plate that is referred to as "gap opening" in this paper, energy dissipation and stress in bolts are investigated and compared to those of reference connections.

3. Modeling method and verification of FE models

To evaluate the accuracy of FE models for both T-stub and end plate bolted connections, the numerical results are compared with experimental results of Specimen 1 (T-stub connection) tested by Popov and Takhirov [8] and 4E-1.5-1.25-24 (end plate connection) tested by Sumner [14] respectively. The experimental specimens of connections were single-sided beam-to-column assemblies that are representative of exterior beam-to-column connections. At T-stub bolted connection, the beam is connected to column flange by two T-stubs and the T-stub stems were welded to the beam and pre-stressed to the beam flanges by means of bolts. The column shear tab was bolted to the beam web. At end plate bolted connection, the beam was connected to end plate by CJP groove and fillet welds and the end plate is attached to column flange by pre-tensioned bolts. Numerical modeling of the connections is carried out by using the following assumptions: the dimensions and geometry of the beam, column and connection components are exactly modeled in accordance with the experimental specimens. Slippage between T-stub stems and beam flange and also column shear tab and beam web is negligible, because these components are connected by welding or pre-tensioned bolts or both. Consequently, these components are modeled continuously. Since end plate and beam are connected by CJP groove and fillet welds, these two parts are considered continuous in the FE model. All components of the connection are modeled using eight-node first-order SOLID45 elements. Fig. 1 shows the FE model and mesh pattern of these connections. This element has plasticity, creep, swelling stress stiffening, large deflection and large strain capabilities and allows orthotropic properties and also pressure and temperature loadings. The geometrical discontinuities are simulated by surface-to-surface contact elements (TARGE170 and CONTA173). Thus, the effect of adjacent surfaces' interaction, including T-stub stem/beam flange, T-stub flanges/end plate bolt nut, column flange/bolt head, bolt hole/bolt shank and effect of friction are modeled using the

Table 1
Material properties used in specimens to validate numerical and experimental results.

Material	Application	Strain	Stress (MPa)
ASTM A36	End plate	0.001276 0.01403 0.153	262 262 476
ASTM A572 Gr50	Beam, column, T-stub	0.00178 0.0196 0.2134	361 361 488
A490	Bolt	0.00386 0.0135 0.0309 0.2	794 1035 1035 1048

mentioned contact elements. Bolt heads and nuts are modeled as hexagonal similar to their actual shape. To consider the frictional forces, Coulomb's coefficient is assumed to be 0.3, which yields the best results. The mechanical properties of all component materials are taken from the experimental specimens mentioned in Table 1. An isotropic multi-linear kinematic hardening rule with a von Mises yielding criterion is applied to simulate plastic deformations of the connection components. This is suitable for simulation of metal plasticity under cyclic loading [15]. The load is applied in two steps. Bolt pre-tension is applied as the first load case by thermal gradient on the bolt shanks to yield equivalent pre-tension force. A displacement is then imposed at the beam tip to generate a bending moment at the connection similar to cyclic loadings on the experimental specimens.

From Fig. 2, it can be seen that similar to experimental specimens, in the FE models, the plastic hinge in the end plate connection formed on the beam at 30 cm from the column face and in the T-stub connection, the slight buckling in the beam web and flanges and yielding of the T-stub flanges is occurred.

Fig. 3 shows the comparison between hysteresis loops of moment at column centerline versus total rotation (M–θ) of the FE model and of the test data for end plate connection and also between load versus displacement (F–Δ) of the FE model and of the test data for T-stub connection. From this figure, in the experimental specimens, the maximum moment at the end plate connection and the maximum applied load of the T-stub connection are 11 703 in. kips and 1535 kN, respectively; while numerical results of the corresponding FE models are 11 094 in. kips and 1441 kN, which are 5.2% and 6.1% different at maximum values. Moreover, according to Fig. 4, the maximum gap opening in the "Specimen 1" is 8 mm, while in the corresponding FE model, it is 8.4 mm. Moment at column centerline versus bolt strain curve in Fig. 5 revealed an approximately similar behavior of the bolt between "4E-1.5-1.25-24" and the corresponding FE model. This figure also represents a reduction in the strain value in the bolt, reaching to about 2×10^{-4} in both specimens. Therefore, it can be seen that the results obtained from finite element models and test data have a good agreement.

4. Finite element models

The deflection as well as bending moment diagram of a moment resisting frame under lateral loads is shown in Fig. 6. As can be

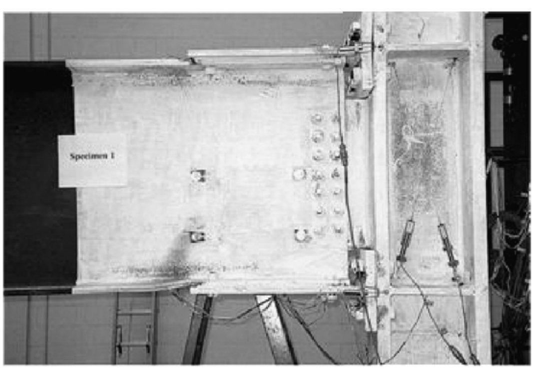

(a) "Specimen1" [8] after the test.

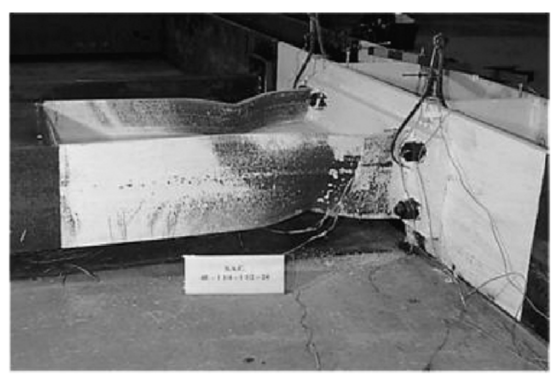

(b) "4E-1.5-1.25-24" [14] after the test.

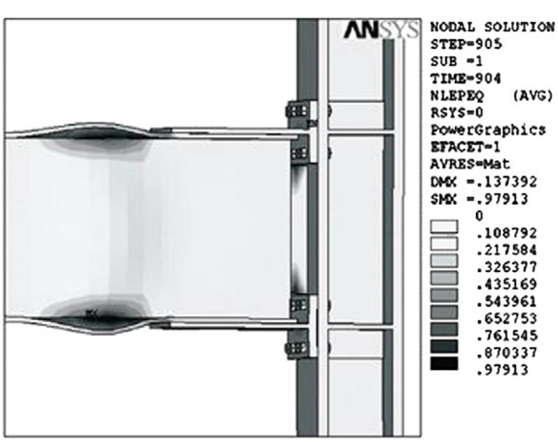

(c) Equivalent plastic strain at final stage of loadings of the "Specimen1" FE model.

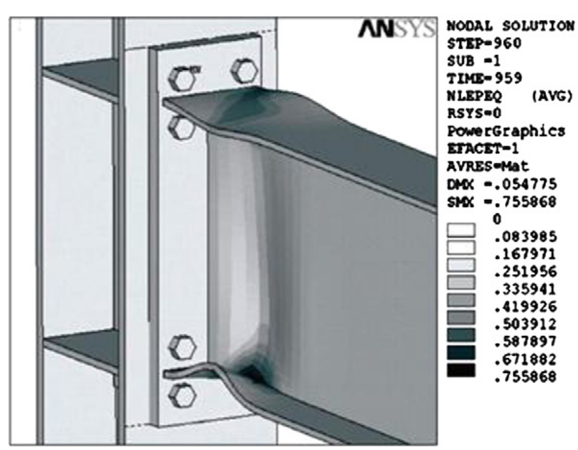

(d) Equivalent plastic strain at final stage of loadings of the "4E-1.5-1.25-24" FE model.

Fig. 2. View of experimental and numerical specimens.

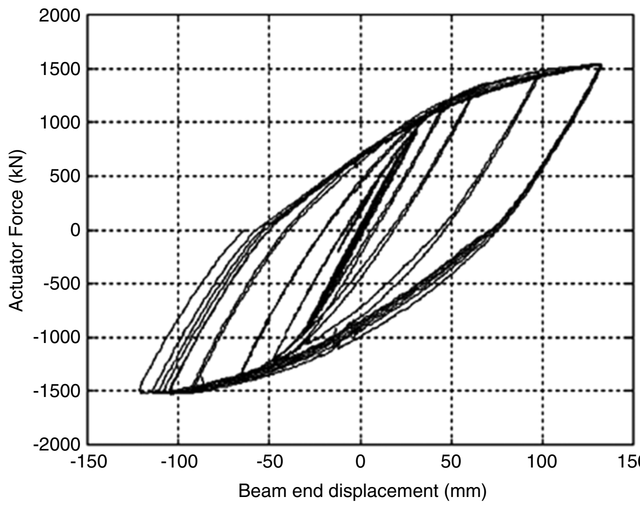

(a) Hysteretic curves for experimental results "Specimen 1".

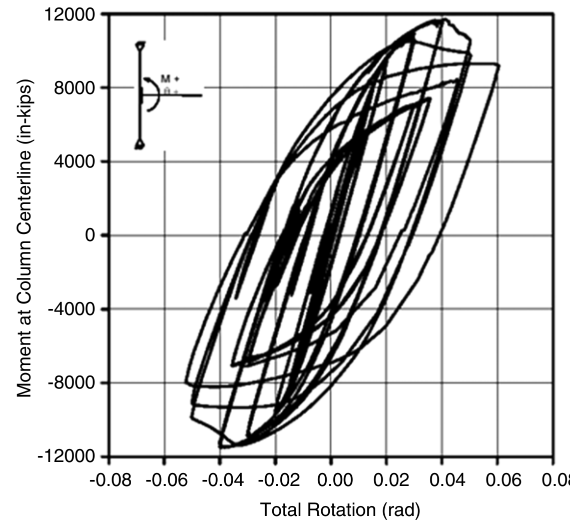

(b) Hysteretic curves for experimental results "4E-1.5-1.25-24".

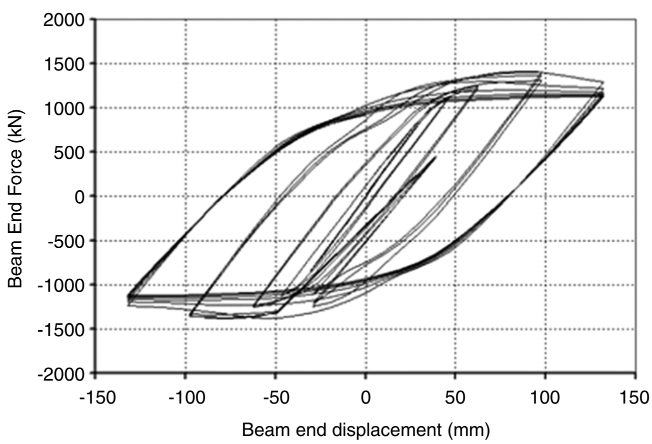

(c) Hysteretic curves for numerical results "Specimen 1".

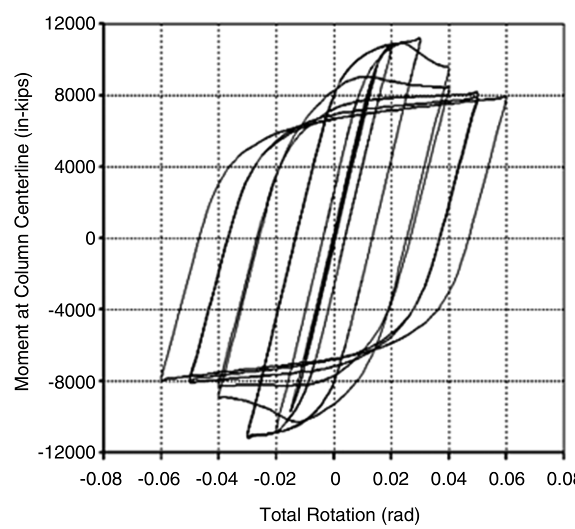

(d) Hysteretic curves for numerical results "4E-1.5-1.25-24".

Fig. 3. F–Δ and M–θ hysteresis curves of numerical and experimental specimens.

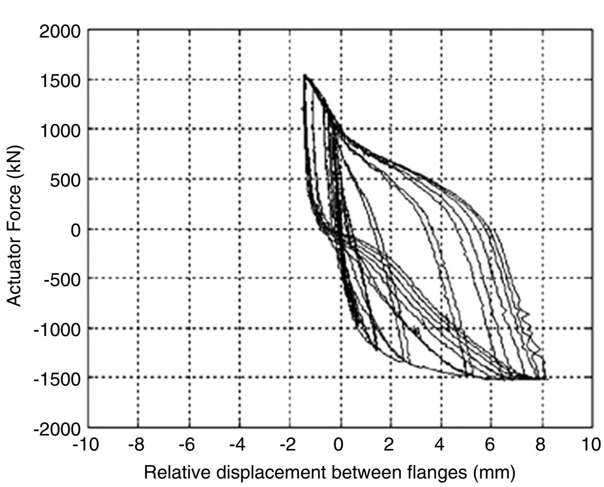

(a) Experimental result of "Specimen 1" [8].

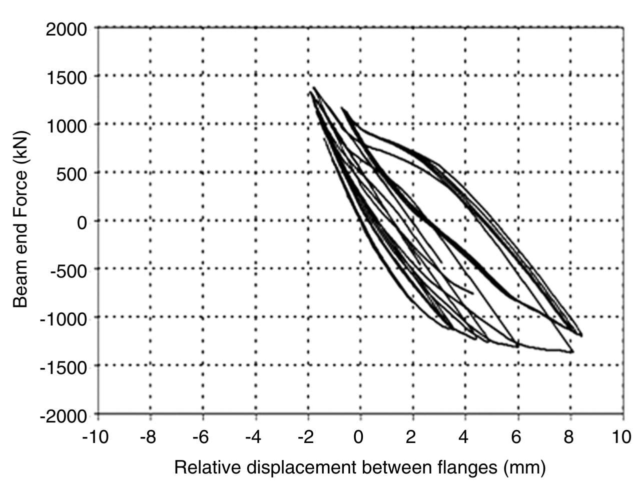

(b) Numerical result of "Specimen 1".

Fig. 4. Relative displacement between column and top T-section flanges.

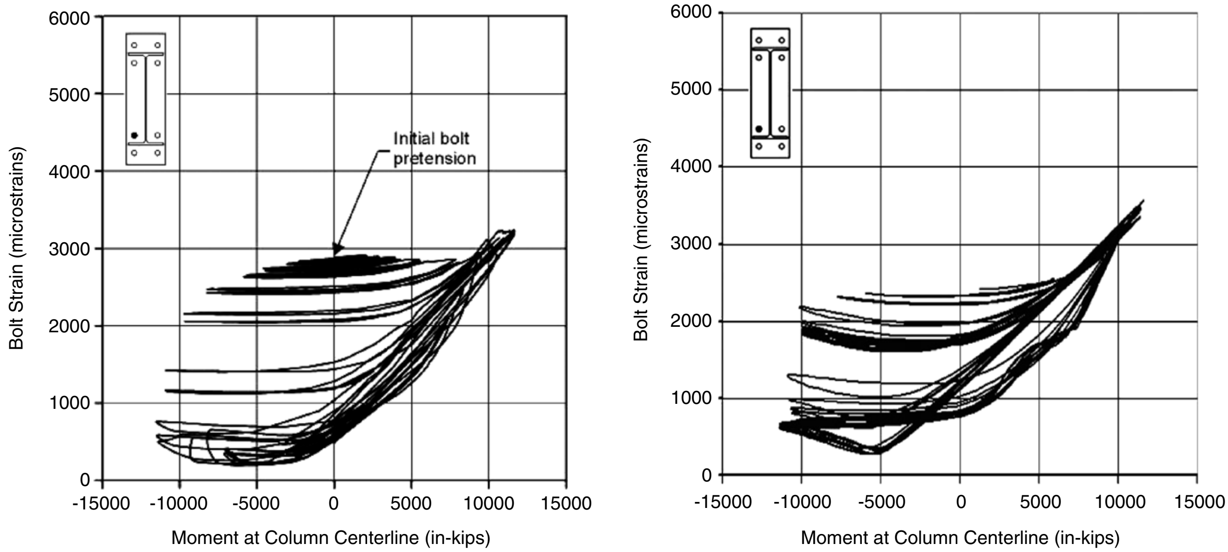

(a) Experimental result of "4E-1.5-1.25-28" [14]. (b) Numerical result of "4E-1.5-1.25-24".

Fig. 5. Bolt strain versus moment at column centerline.

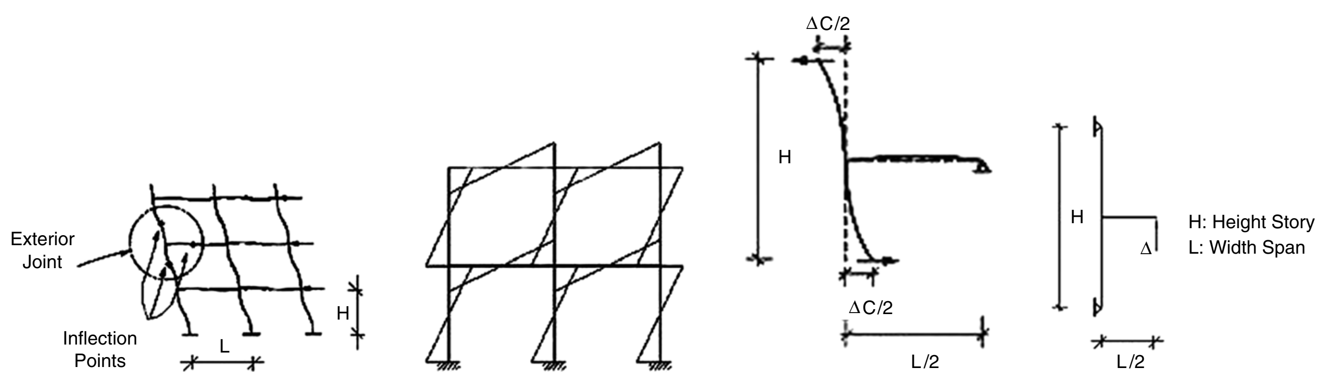

(a) Deflection diagram of the moment resisting frame. (b) Moment diagram. (c) Exterior connection separated from inflection point. (d) Applied substructure in numerical study.

Fig. 6. Moment resisting frame under lateral loads.

seen, the bending moment at the midspan of the beam and the column is equal to zero and the midpoint of the beam and the column under lateral loads is the inflection point. Contrary to bending moment, the value of the shear force at the inflection point is not equal to zero. Since the modeling of the frame is very difficult and time consuming, the connection can be considered separately from the inflection point in order to study the behavior of the moment resisting connections. The pinned or roller supports can be applied to bear the shear forces at these points and then the substructure can be modeled and analyzed as it is shown in Fig. 6.

The connection models are single-sided beam-to-column assemblies. They are composed of IPE550 (4.5 m length) beams and IPB450 (3 m length) columns. T-stubs are cut from IPB500 sections. The stress–strain relation for all connection components is represented using a multi-linear constitutive model in Table 2.

As is shown in Fig. 7 and presented in detail in Table 3, the SAC standard loadings are applied to the specimens in accordance with FEMA350 [16]. In order to investigate the influence of the bolt arrangement variation (b and c parameters in Fig. 8), TSR (T-stub Reference) and EPR (End Plate Reference) are designed with identical beam and column sections based on AISC [17,18] as the reference specimens. Specimens that are generally named as

Table 2
Material properties used in FE modeling.

Material	Application	Strain	Stress (MPa)
ST37	Beam, column, end plate, T-stub	0.001143 0.02 0.18 0.2 0.35	240 240 360 370 370
A490	Bolt	0.00386 0.0135 0.0309 0.2	794 1035 1035 1048

TS$\pm\Delta c$ and EP$\pm\Delta c$ belong to group A. They are developed to study the influence of horizontal distance between bolts and centerline of the beam web (c). Moreover, the specimens that are generally named as TS$\pm\Delta b$ and EP$\pm\Delta b$ belong to group B and are developed to investigate the effect of vertical distance between bolts and beam flange (b). The signs $+\Delta c$ and $+\Delta b$ represent any increase in horizontal and vertical distance of bolts and the signs $-\Delta c$ and $-\Delta b$ represent any decrease in such a distance compared with that of the corresponding reference specimens, respectively. The details of the specimens are presented in Table 4 and Fig. 9. It should be

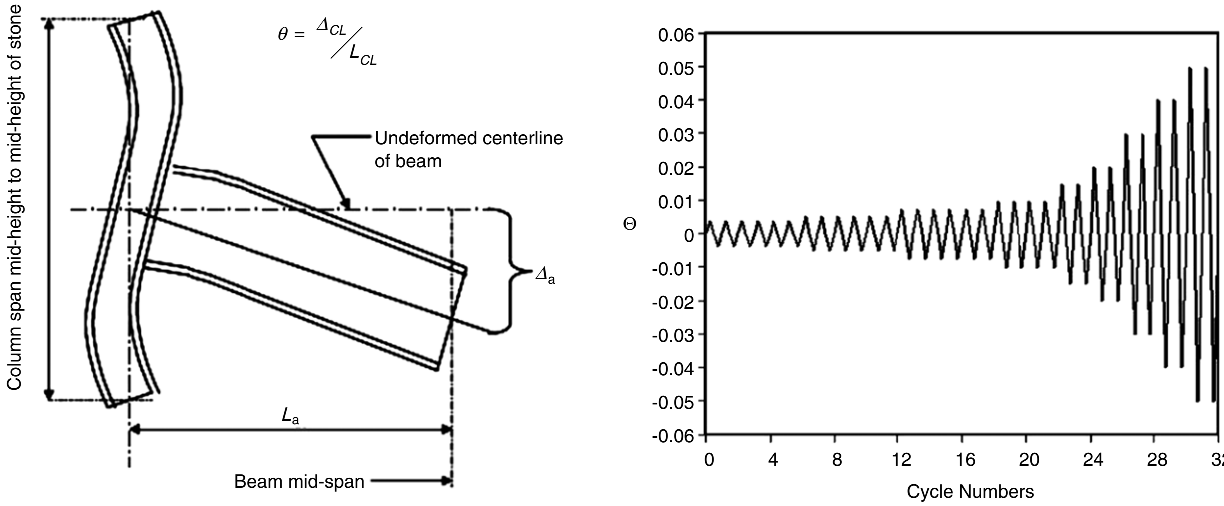

Fig. 7. FEMA/SAC2000 loading protocol in accordance with FEMA350 [16].

Table 3
Details of the cyclic loading according to SAC standard.

Load step	Peak deformation, θ (rad.)	Number of cycles	Beam end displacement (cm)
1	0.00375	6	0.95
2	0.005	6	1.26
3	0.0075	6	1.89
4	0.01	4	2.53
5	0.015	2	3.79
6	0.02	2	5.05
7	0.03	2	7.58
8	0.04	2	10.1
9	0.05	2	12.63

noted that the variation of bolt arrangement is considered based on possible maximum displacement so that the connections can be assembled properly.

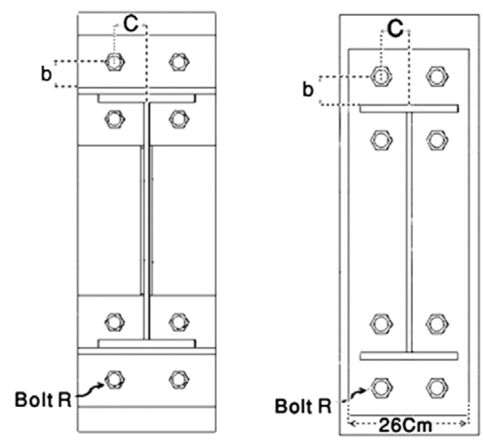

Fig. 8. Introduction of (b) and (c) parameters.

5. Numerical results

The numerical results are presented in Tables 5 and 6 which are discussed in three separated sections. The influence of horizontal and vertical arrangement of bolts on cyclic behavior of T-stub and end plate bolted connections is considered in the first and second sections. Thereafter, the cyclic behavior of the connections is studied by comparing the numerical results of TSR with EPR specimens.

5.1. Effect of horizontal distance between bolts and centerline of the beam web (c parameter)

Considering the numerical results of group A specimens, the following results can be implied.

Fig. 10 shows the equivalent plastic strain of the specimens at the final stage of loading. It can be seen that the failure is occurred by plastic hinge formation in the beam in each of the three end plate connections. Furthermore, it shows no dependence of

Table 4
Summary of numerical specimen details.

Group	Specimen	Number of bolts around any flange	Bolt diameter D_b (cm)	a (cm)	b (cm)	c (cm)	End plate thickness t_{Pl} (cm)	T-stub flange thickness (cm)	Pre-stressing S_P (MPa)
Ref	TSR	4	2.7	5.8	5.475	7	–	2.8	570
	EPR	4	3	6	6	6	3.3	–	570
A	TS+3c	4	2.7	5.8	5.475	10	–	2.8	570
	TS−3c	4	2.7	5.8	5.475	4	–	2.8	570
	EP+1.5c	4	3	6	6	7.5	3.3	–	570
	EP−1.5c	4	3	6	6	4.5	3.3	–	570
B	TS+1.5b	4	2.7	4.3	6.975	7	–	2.8	570
	TS+2b	4	2.7	3.8	7.475	7	–	2.8	570
	TS−1b	4	2.7	6.8	4.475	7	–	2.8	570
	EP+2b	4	3	4	8	6	3.3	–	570
	EP+3b	4	3	3	9	6	3.3	–	570
	EP−1b	4	3	7	5	6	3.3	–	570

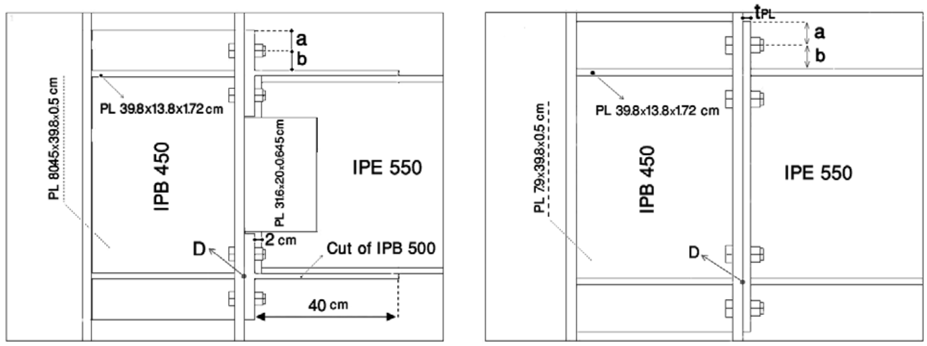

(a) T-stub connection. (b) End plate connection.

Fig. 9. Details of numerical specimens.

Table 5
Finite element results: Moment resistance capacity, initial rotational stiffness and failure mode.

Group	Specimens	$M_{\max}$ (kN m)	$\frac{M_{\max}}{M_{\max(EPR/TSR)}}$	M_y (kN m)	θ_y (rad. $\times 10^{-4}$)	$R_{in} = \frac{M_y}{\theta_y}$ (MN m/rad.)	$\frac{R_{in}}{R_{in(EPR/TSR)}}$	[a]F
Ref	TSR	931	1.000	805	75	107.3	1.00	a
	EPR	766	1.000	716	75	95.5	1.00	a
A	TS+3*c*	930	0.999	799	75	106.5	0.99	a
	TS−3*c*	650	0.700	390	43	90.7	0.85	b
	EP+1.5*c*	766	1.000	704	75	93.9	0.98	a
	EP−1.5*c*	766	1.000	723	75	96.4	1.01	a
B	TS+1.5*b*	926	0.994	811	8	101.4	0.94	a
	TS+2*b*	908	0.975	740	82	90.2	0.84	c
	TS−1*b*	932	1.001	838	75	111.7	1.04	a
	EP+2*b*	767	1.001	711	76	93.6	0.98	a
	EP+3*b*	775	1.011	685	78	87.9	0.92	d
	EP−1*b*	765	0.998	718	74	98.1	1.02	a

[a] Failure mode
a Plastic hinge in the beam.
b Plastic hinge in the T-stub stem.
c Fracture in bottom column bolts at 0.03 rad.
d Fracture in bottom column bolts at 0.05 rad.

Table 6
Finite element results: energy dissipation, the maximum gap opening and residual pre-stressing of *R* bolt.

Group	Specimens	[a]NP	[b]E_{total} (kJ)	$\frac{E_{\text{total}}}{E_{\text{total(EPR/TSR)}}}$	E_{beam} (%)	E_{EEP} or E_{Tee} (%)	$E_{\text{Shera Tab}}$ (%)	$\text{Gap}_{\max}(D)$ (mm)	$\frac{\text{Gap}_{\max}}{\text{Gap}_{\max(EPR/TSR)}}$	$\frac{S_{B(\min)}}{S_P}$	$\frac{S_{B(\min)}}{S_{B(\min EPR/TSR)}}$
Ref	TSR	13	670	1.000	81	16	2	4.8	1.00	0.34	1.00
	EPR	14	655	1.000	100	0	–	1.3	1.00	0.93	1.00
A	TS+3*c*	12	672	1.003	79	17	2	5.7	1.18	0.33	0.98
	TS−3*c*	19	487	0.730	0	83	16	3.3	0.68	0.32	0.96
	EP+1.5*c*	14	624	0.950	100	0	–	1.7	1.38	0.88	0.95
	EP−1.5*c*	14	673	1.030	100	0	–	0.8	0.61	0.92	0.99
B	TS+1.5*b*	13	586	0.870	63	30	4	9.0	1.85	0.23	0.67
	TS+2*b*	8	139	0.210	11	73	13	11.8	2.42	0.22	0.64
	TS−1*b*	13	725	1.080	94	5	0.5	2.1	0.44	0.58	1.71
	EP+2*b*	13	633	0.960	99	0.9	–	1.8	1.43	0.87	0.93
	EP+3*b*	11	534	0.81	74	22	–	8.0	6.35	0.37	0.40
	EP−1*b*	14	647	0.99	100	0	–	1.03	0.82	0.95	1.02

[a] Number of inelastic excursions.
[b] Total energy dissipated (KJ).

global behavior of such connections to variation of this parameter. However, by comparing T-stub connections with TSR, just in TS−3*c* the failure is occurred by plastic hinge formation in the T-stub stem instead of that in the beam (see Fig. 11). It can be attributed to the increase in the stiffness of the connection adjacent to T-stub flange and consequently, the increase in deflections and plasticity in T-stub stem.

Fig. 12 shows the moment versus total rotation hysteresis loops of the group A specimens. It revealed that just in TS−3*c*, the moment capacity is reduced by 30% compared with that of TSR. The reason can be the change of failure mode in this specimen.

The resisting moment and corresponding rotation at the structure yield point is calculated based on moment versus total rotation hysteresis envelope shown in Fig. 13. After calculating the initial rotational stiffness of the connection ($R_{\text{ini}} = M_y/\theta_y$), it is found that just in TS−3*c*, the initial rotational stiffness is decreased by 15% compared to that of TSR.

Considering the diagrams of the gap opening at node D versus total rotation, it is shown that decreasing the distance between bolts and beam web in EP−1.5*c* and TS−3*c* will decrease the maximum gap opening by 39% and 32% compared with that of the corresponding reference specimens respectively, and increasing the distance between the bolts and beam web will increase it by 38% and 18% in EP+1.5*c* and TS+3*c* respectively. These curves for the reference specimens are shown in Fig. 14.

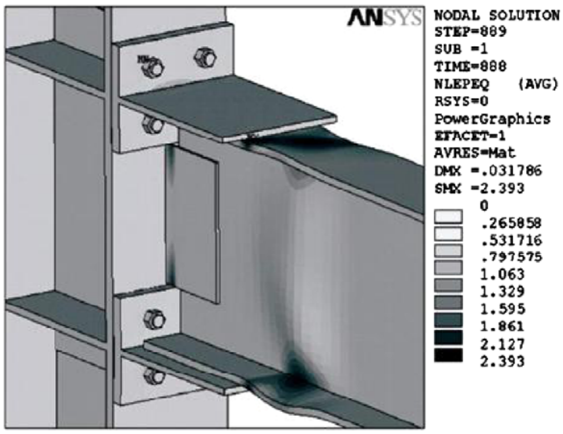

(a) TSR.

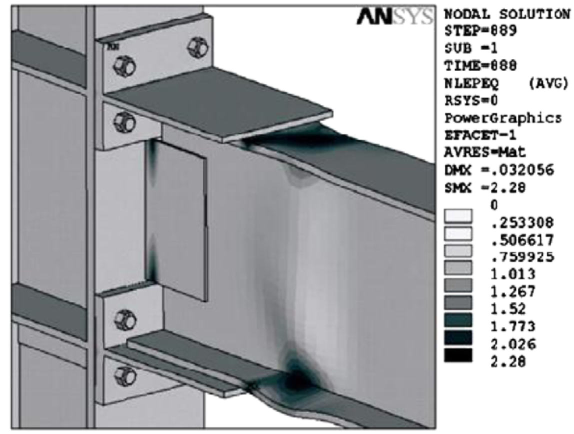

(b) TS + 3c.

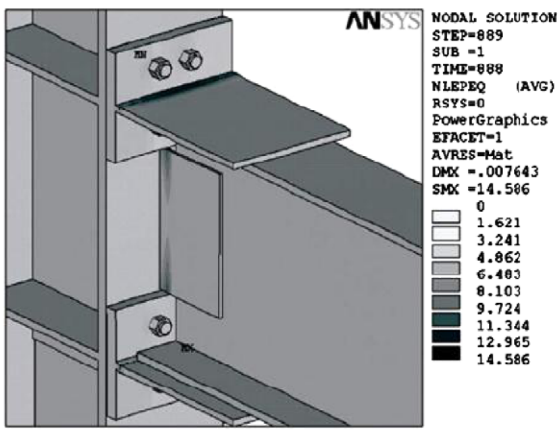

(c) TS − 3c.

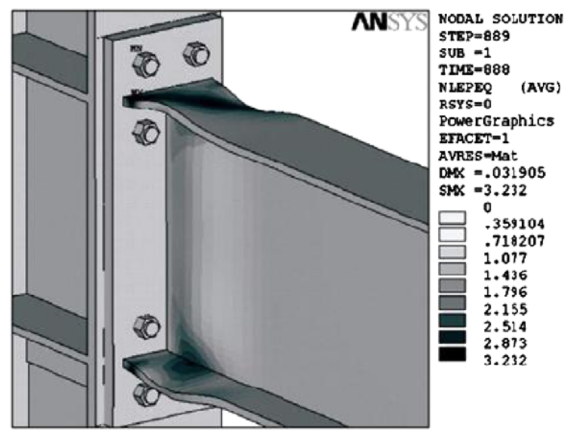

(d) EPR.

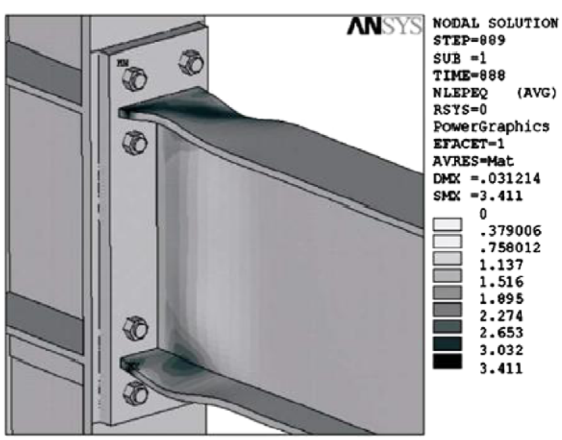

(e) EP + 1.5c.

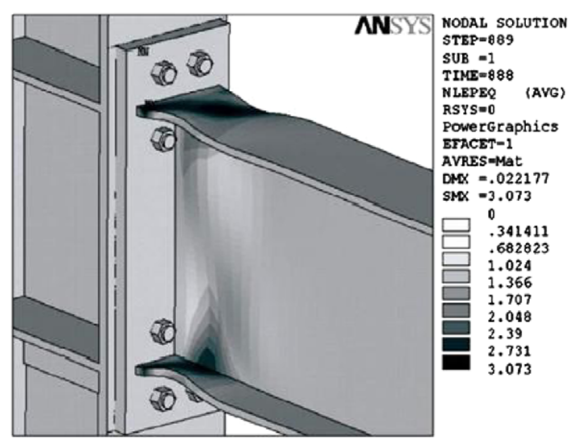

(f) EP − 1.5c.

Fig. 10. Equivalent plastic strain EPEQ at the final stage of loading for reference and group A specimens.

However, the failure mode in all end plate connections are yielding, local buckling of the beam flange and web and thus, no considerable yielding is observed in the end plate at the final stage of loading (see Fig. 10). Therefore, all of the energy is dissipated by the beam. In the T-stub connections, just in TS−3c, changing of failure mode results in the increase of T-stub contribution in energy dissipation by 67% compared to that of TSR. Moreover, in contrast to TSR which the beam contributed in energy dissipation about 81%, in TS−3c the beam remains elastic and do not have any contribution in energy dissipation.

The energy dissipation characteristic of group A connections is presented in Fig. 15. The total energy dissipation is increased by 3% in EP−1.5c compared with that of EPR. The reason could be attributed to the stiffening of the connection and consequently, the deflection and further plasticity of the beam at the same number of inelastic cycles. Furthermore, reducing the distance between the bolts and the beam web in TS−3c, despite the fact that increases the number of inelastic cycles will decrease the total energy dissipation about 27% compared with that of TSR. The reason could be the change of failure mode and elastic remaining of the beam. Moreover, increasing the distance between the bolts and beam web in EP+1.5c and TS+3c will decrease the total energy dissipation by 5% and 2% respectively compared with that of the corresponding reference specimens.

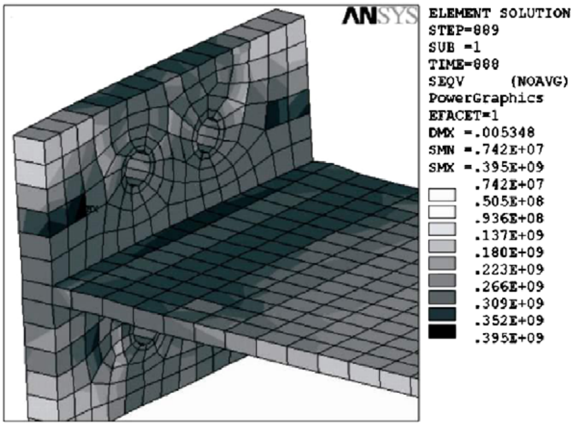

Fig. 11. Von Mises stress in the top T-stub at the final stage of loading for TS−3*c*.

Considering the diagrams of the gap opening at node D versus total rotation, it is found that the increase of the distance between the bolts and the beam flange in EP+2*b*, EP+3*b*, TS+1.5*b*, and TS+2*b* increases the maximum gap opening by 1.43, 6.35, 1.85, and 2.42 times respectively compared with that of the corresponding reference specimens. Moreover, decreasing the distance of the bolts and the beam flange in EP−1*b* and TS−1*b* decreases the maximum gap opening by 18% and 56% compared with that of the corresponding reference specimens.

$S_{B\ \min}/S_{B\ \min\ R}$ ratio in Table 6 represents the ratio of the minimum axial stress of the bolt R during the loading in specimens to that of the corresponding reference specimens. It shows that the variation of horizontal distance between bolts has negligible effect on maximum decrease of axial stress in the bolts during the loading. Fig. 16 shows the variation trend of pre-stressing in bolt R during the loading for the reference and group A specimens.

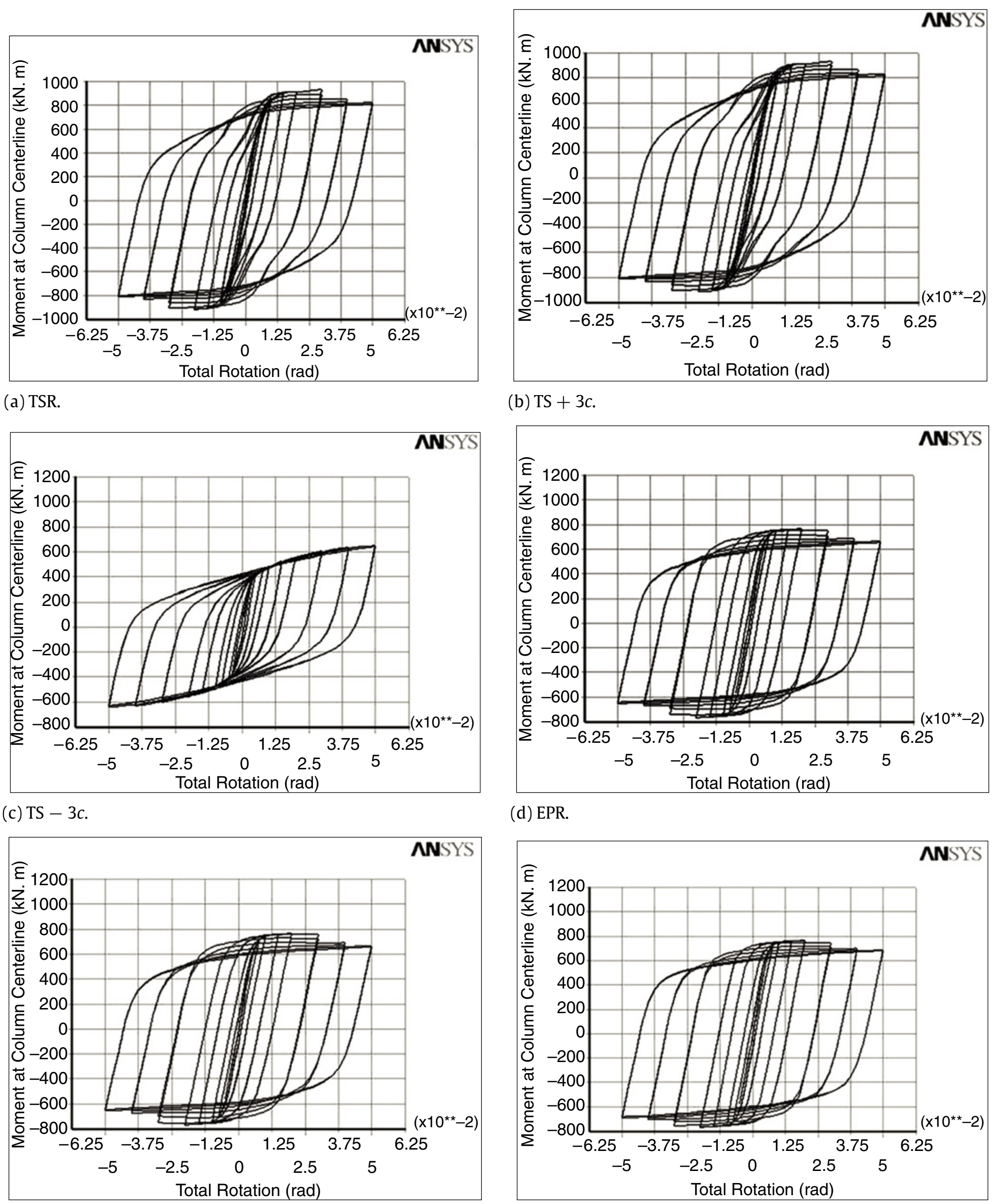

(a) TSR.

(b) TS + 3*c*.

(c) TS − 3*c*.

(d) EPR.

(e) EP + 1.5*c*.

(f) EP − 1.5*c*.

Fig. 12. Moment versus total rotation hysteresis loops for reference and group A specimens.

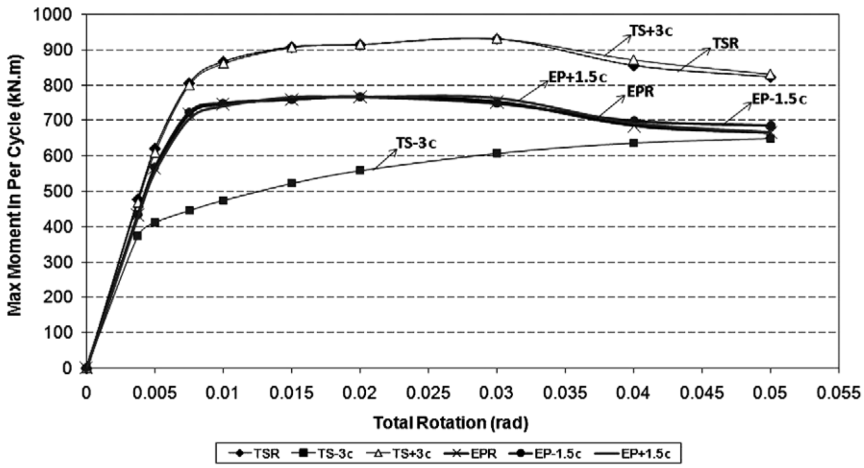

Fig. 13. Moment versus total rotation hysteresis envelope of the reference and group A specimens.

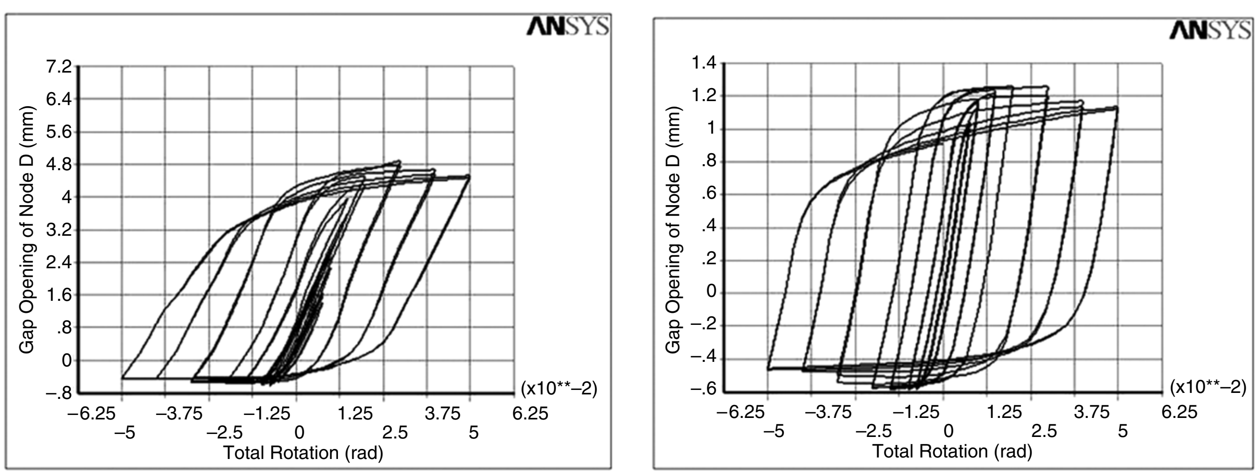

(a) TSR.

(b) EPR.

Fig. 14. Gap opening at node D versus total rotation of the reference specimens.

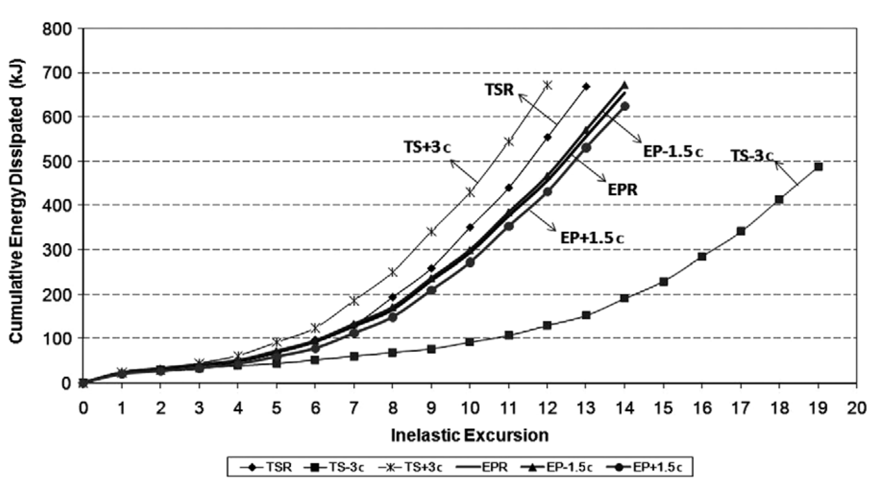

Fig. 15. The energy dissipated by connection and beam assembly in reference and group A specimens.

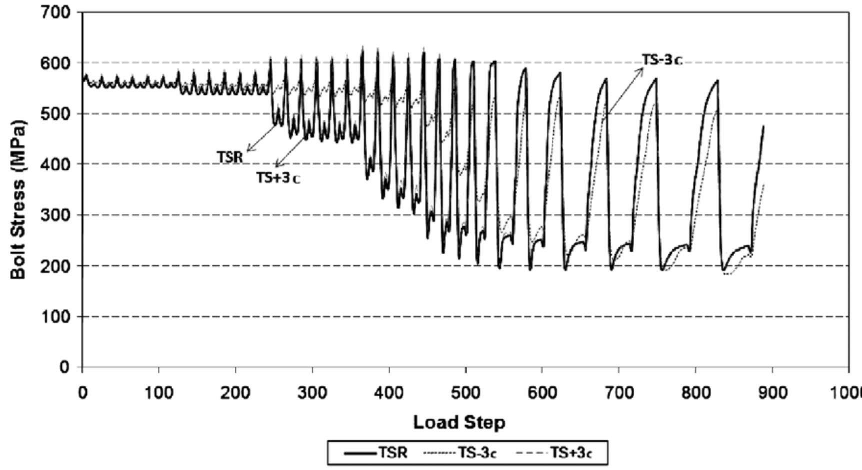

(a) T-stub connections.

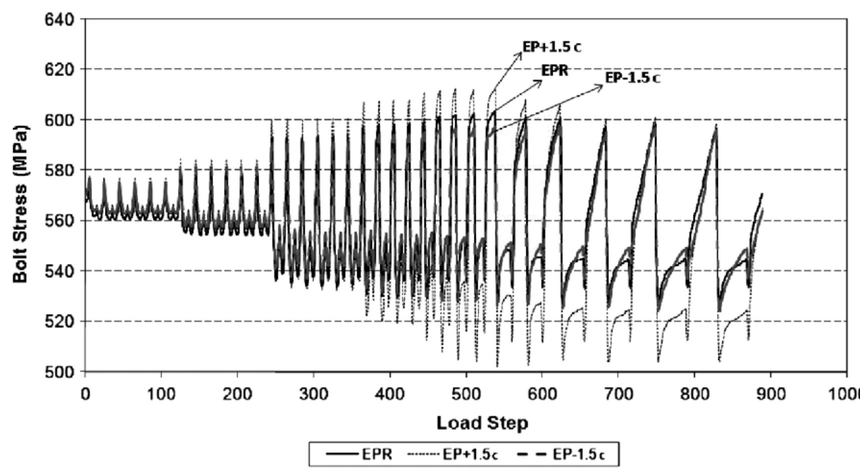

(b) End plate connections.

Fig. 16. Variation of pre-stressing in bolt R during the loading stages for the reference and group A specimens.

5.2. Effect of vertical distance between bolts and beam flange (b parameter)

Considering the numerical results obtained from group B specimens, the following points may be noted.

The equivalent plastic strain of the group B specimens at the final stage of loading is shown in Fig. 17. Comparing the end plate connections and EPR connection, it can be seen that just in EP+3*b* the failure is occurred by fracture of the bottom bolts at the first cycle of 0.05 rad. instead of plastic hinge formation in the beam. Therefore, by comparing the T-stub and TSR connection, it can be observed that just in TS+2*b* failure is occurred by fracture of the bottom bolts at the second cycle of 0.03 rad. instead of plastic hinge formation in the beam. The main factors affecting the bolt fracture in these connections are the increase in bending deflections and consequently, significant decreases in pre-stressing force.

Von Mises stress in the bottom bolts in these connections is shown in Fig. 18. It should be noted that the decrease in plasticity at the beam and consequently, its increase at the end plate or T-stub flange will occur due to the increase in distance between bolt and beam flange in both types of connections.

Fig. 19 shows the moment versus total rotation hysteresis loops of group B specimens. It reveals that variation of this parameter has negligible effect on moment capacity. Moreover, it shows that the increase in vertical distance between the bolts and the beam flange produces hysteresis loops with more pinching, especially in T-stub connections. The pinching of the hysteretic loops indicates plasticity and permanent deflection increase at the end plate or the T-stub flange.

The initial rotational stiffness of the connection is calculated based on moment versus total rotation hysteresis envelope (see Fig. 20). It is found that the increase in vertical distance between the bolts and the beam flange in EP+2*b*, EP+3*b*, TS+1.5*b*, and TS+2*b* decreases the initial rotational stiffness by 2%, 8%, 6%, and 16% compared with that of the corresponding reference specimens. On the contrary, the decrease in vertical distance between the bolts and the beam flange in EP−1*b* and TS−1*b* increases the initial rotational stiffness by 2% and 4% compared with that of the corresponding reference specimens.

The energy dissipation characteristic of group B connections is shown in Fig. 21. The energy dissipation in EP+2*b*, EP+3*b*, TS+1.5*b*, and TS+2*b* respectively is 4%, 9%, 13%, and 79% lower than that of the corresponding reference specimens. It is also evident that the increase in the distance between bolts and the beam flange in these connections decreases total energy dissipation. The reason could be attributed to the increase of plasticity of the end plate and T-stub and consequently, decrease of the beam contribution in energy dissipation. Similarly, the end plate for EP+3*b* portion in total energy dissipation is 22%, while it remained elastic in EPR. Furthermore, the T-stubs of TS+1.5*b* and TS+2*b* contributed about 30% and 73% respectively in total energy dissipation, while their proportion is 16% in TSR. It should be noted that TS+2*b* resisted few

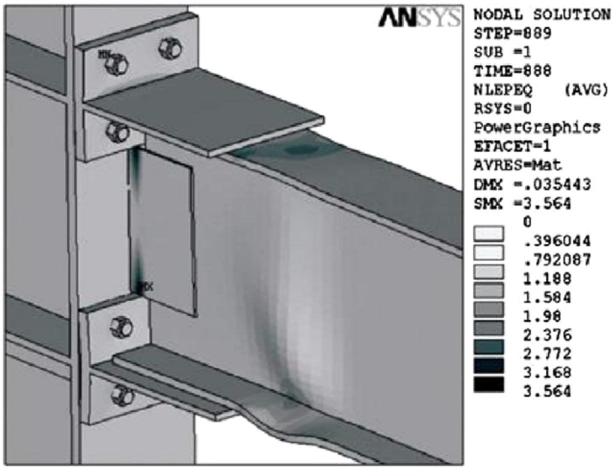

(a) TS + 1.5*b*.

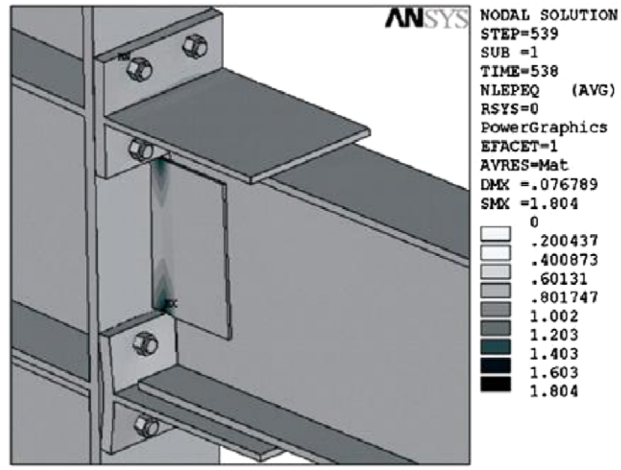

(b) TS + 2*b*.

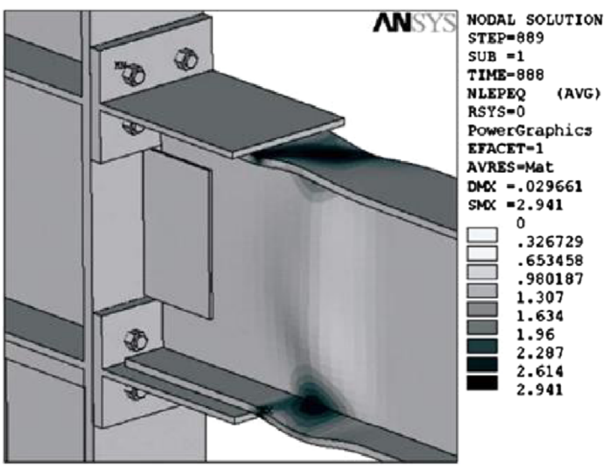

(c) TS − 1*b*.

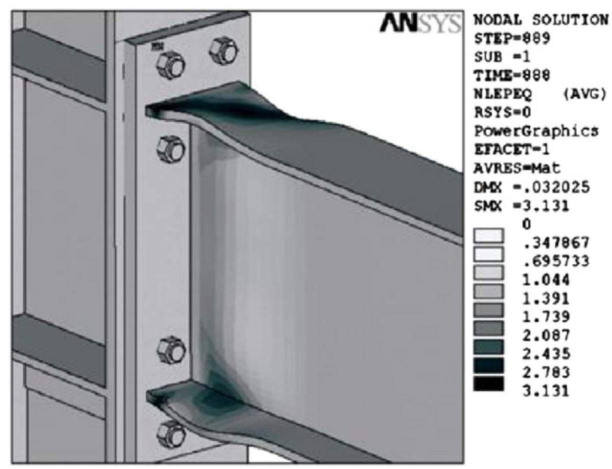

(d) EP + 2*b*.

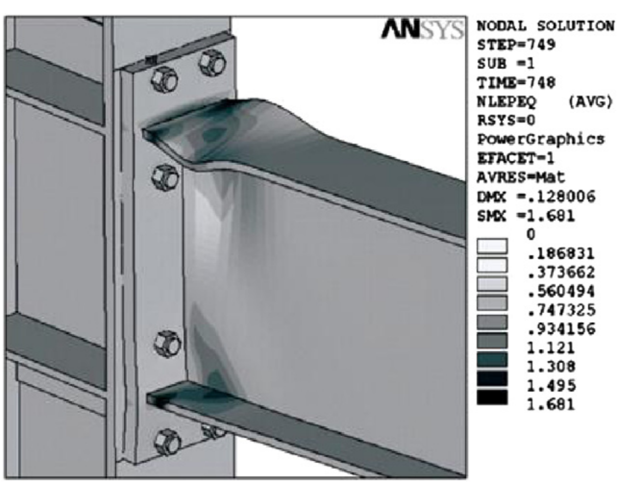

(e) EP + 3*b*.

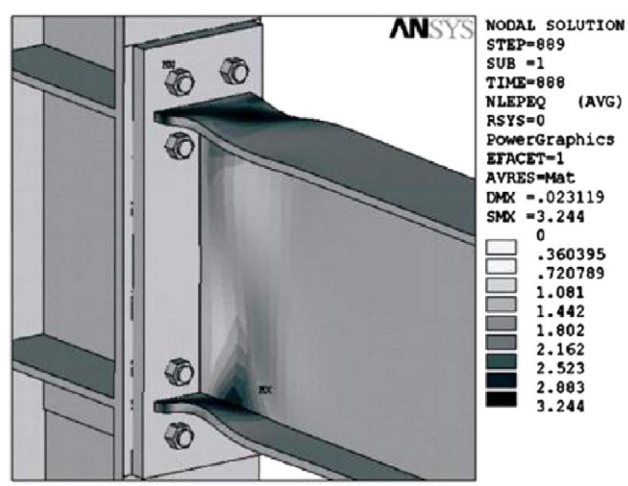

(f) EP − 1*b*.

Fig. 17. Equivalent plastic strain EPEQ at the final stage of loading for group B specimens.

inelastic cycles that resulted in significant decrease in total energy dissipation because of premature failure.

$S_{B\,\min}/S_{B\,\min\,R}$ ratio in Table 6 reveals that the increase in the distance between bolts and the beam flange caused more decreases in pre-stressing of the bolts during the loading. Fig. 22 shows the variation trend of pre-stressing of bolt R during the loading for the reference and group B specimens.

5.3. Comparison of the numerical results of the reference specimens

After comparing the cyclic behavior of the reference specimens, following items can be inferred.

Figs. 13 and 20 show moment versus total rotation hysteresis envelope for TSR and EPR. According to these figures, it is found that the moment capacity of the T-stub connection higher than

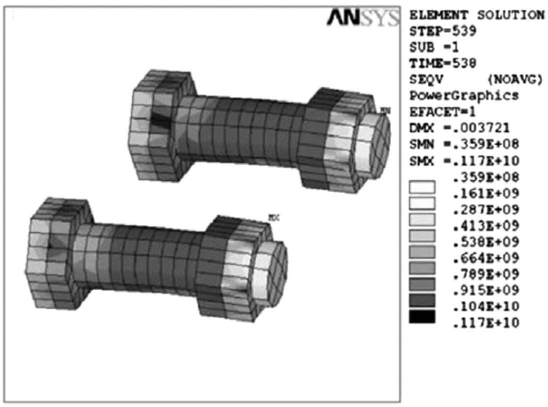

(a) TS + 2*b*.

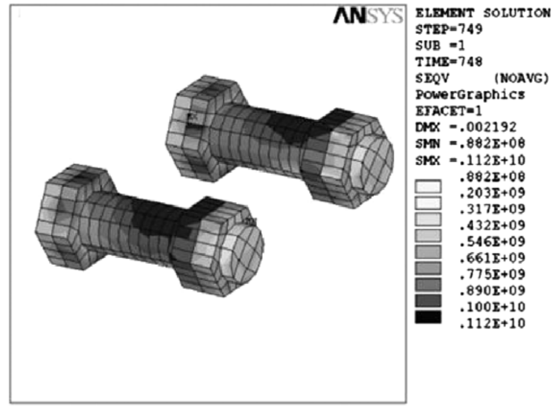

(b) EP + 3*b*.

Fig. 18. Von Mises stress in the bottom bolts of the connection at the final stage of loading for TS+2*b* and EP+3*b* (Pa).

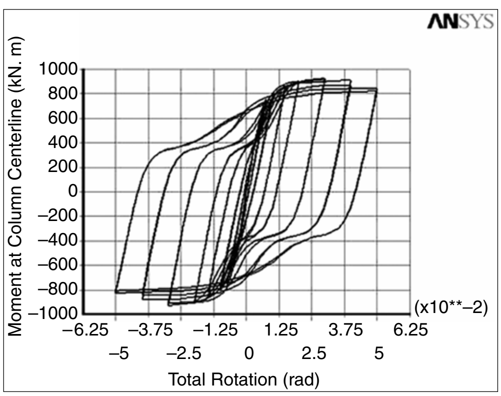

(a) TS + 1.5*b*.

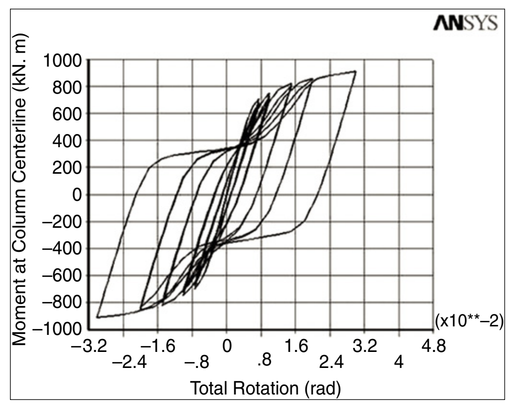

(b) TS + 2*b*.

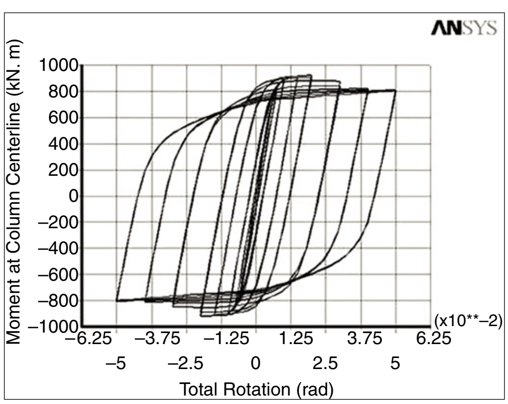

(c) TS − 1*b*.

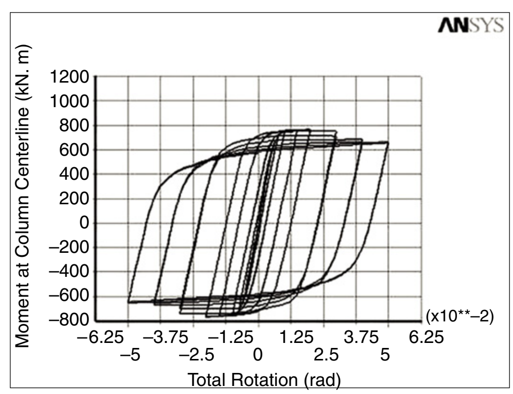

(d) EP + 2*b*.

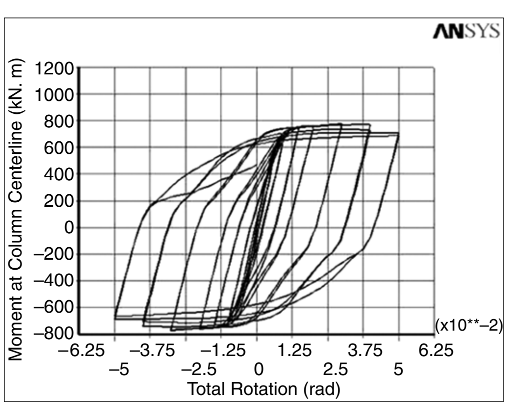

(e) EP + 3*b*.

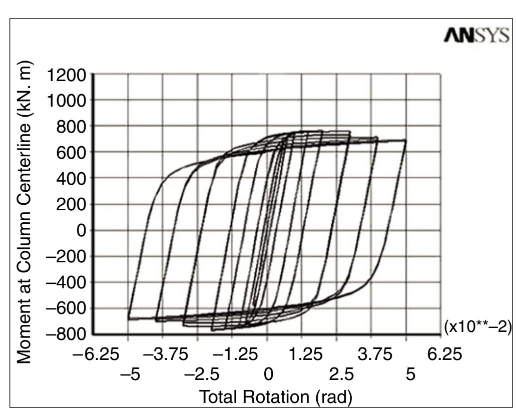

(f) EP − 1*b*.

Fig. 19. Moment versus total rotation hysteresis loops at group B specimens.

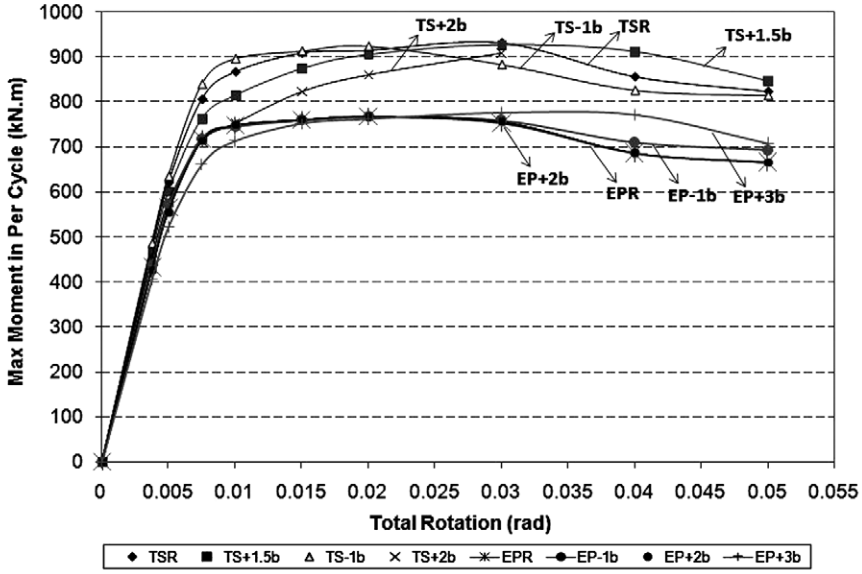

Fig. 20. Moment versus total rotation hysteresis envelope of the reference and group B specimens.

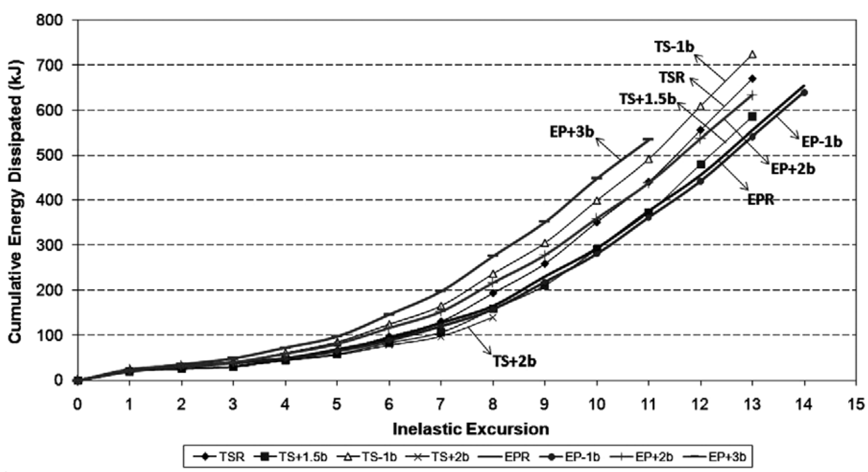

Fig. 21. The energy dissipated by connection and beam assembly in the reference and group B specimens.

end plate connection about 21%. Moreover, the maximum resisting moment in T-stub and end plate connections is obtained at 0.03 and 0.02 rad., respectively. It should be noted that the initial rotational stiffness of the T-stub connection is higher than end plate connection about 12%.

In Figs. 16 and 21, the diagrams show that the dissipated energies in TSR and EPR are rather the same. The end plate remained elastic during the loading and all of the energy is dissipated by the beam, whereas 16% of total energy is dissipated by the T-stubs. It should be noted that FEMA350 believes that end plate connections should be designed in a way that yielding occurs either as a combination of beam flexure and panel zone yielding or as beam flexure alone. The end plate, bolts and welds must be designed so that yielding does not occur in these components.

$S_{B\,\min}/S_p$ ratio in Table 6 represents the ratio of minimum axial stress of bolt R during the loading to initial pre-stressing. It shows that the initial pre-stressing of bolts decreased in all specimens during the loading. Similarly, the initial pre-stressing of bolt R in TSR and EPR decreased by 66% and 7%, respectively. The diagrams of axial force in bolt R versus moment at column centerline is presented for the reference specimens in Fig. 23. They show the variation of pre-tension force during the loading. It can be stated that the pre-tension force in T-stub connection is decreased considerably compared with that of end plate connection. This means that negligible pre-tension force remained in T-stub connection at the end of the loading while this value is considerable in end plate connection.

6. Conclusions

In this study, the cyclic behavior of end plate and T-stub beam-to-column bolted connections is analyzed and compared for different arrangements of bolts using finite element analysis. The results of numerical models showed a good agreement with the test data. The conclusions are:

- The failure is occurred by the formation of plastic hinge in the beam of TSR and EPR. Bolt arrangement variation results in the change of failure mode to brittle fracture of bolts in TS+2*b* and EP+3*b* and also to form plastic hinge in T-stub stem in TS−3*c*.
- Bolt arrangement variation has insignificant effect on the moment capacity of connections except the TS−3*c* connection. In this specimen, the moment capacity is become 30% less than TSR. It could be attributed to the failure mode change and as a result, the beam is remained elastic.

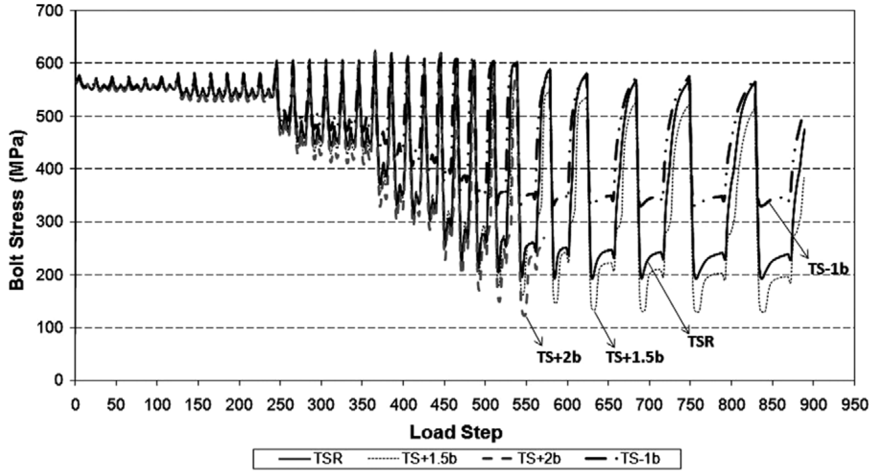

(a) T-stub connections.

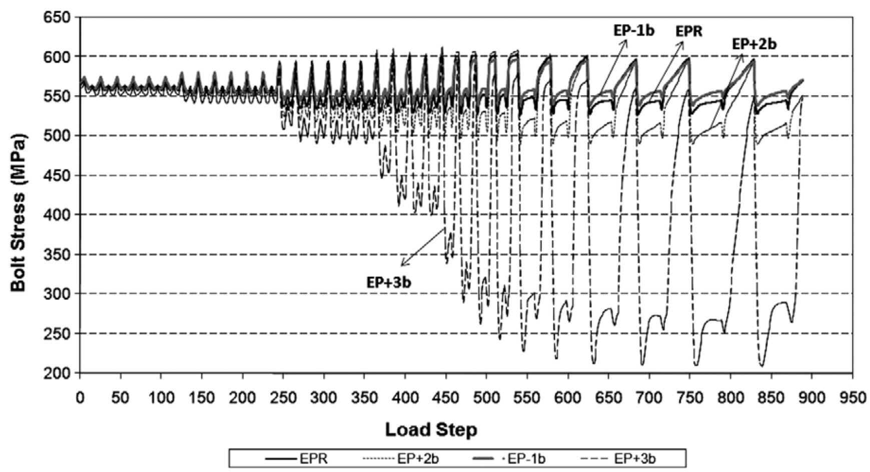

(b) End plate connections.

Fig. 22. Variation of pre-stressing in bolt R during loading stages for reference and group B specimens.

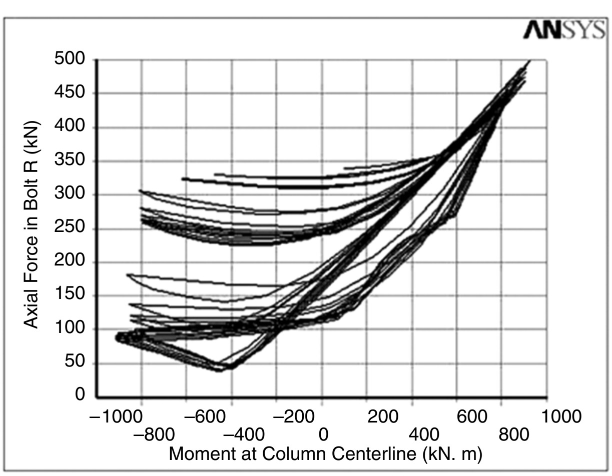

(a) TSR.

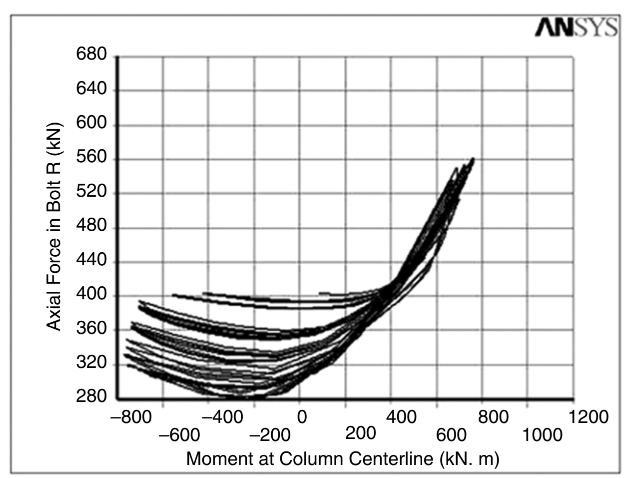

(b) EPR.

Fig. 23. Variation of pre-tension force in bolt R versus moment at column centerline of reference specimens.

- The increase in vertical distance between the bolts and the beam flange produces hysteresis loops with more pinching, especially in T-stub connections. Pinching of the hysteretic loops indicates the increasing in plasticity and deflection of the end plate or the T-stub flange.
- Increasing the distance between the bolts and the beam web or beam flange in such connections results in a reduction of initial rotational stiffness and an increase in maximum gap opening. For example, in TS+2*b* and EP+3*b*, the initial rotational stiffness decreases by 16% and 8% and the maximum gap opening

increases by 242% and 635%, respectively, compared with those of the corresponding reference specimens.

- Increasing the distance between the bolts and the beam flange decreases total energy dissipation. However, it increases contribution of connection components (i.e. end plate or T-stubs) to energy dissipation.
- The moment capacity of TSR is about 21% higher than EPR, while they are designed in a same beam and column section based on AISC. However, their energy dissipation is approximately the same. It should be noted that the T-stubs contribute in energy dissipation, while the end plate is remained elastic during the loading and does not contribute in energy dissipation.
- The probability of failure mode change in T-stub connection is higher than that of end plate connection under cyclic loading due to the bolt arrangement change. Therefore, the end plate connection is suggested for conditions where the imperfection in construction is probable.

References

[1] Adey BT, Grondin GY, Cheng JJR. Cyclic loading of end plate moment connections. Canadian Journal of Civil Engineering 2000;27:683–701.
[2] AISC Special Task Committee on the Northridge Earthquake . Assessing steel damage in the Northridge earthquake. Modern Steel Construction 1994;34(5): 14–8.
[3] Miller DK. Lessons learned from the Northridge earthquake. Engineering Structures 1998;20(4–6):249–60.
[4] Tremblay R, Timler P, Bruneau M, Filiatrault A. Performance of steel structures during the 1994 Northridge earthquake. Canadian Journal of Civil Engineering 1995;22(2):338–60.
[5] Tremblay R, Bruneau M, Nakashima M, Prion HGL, Filliatrault A, DeVall R. Seismic design of steelbuildings: lessons from the 1995 Hyogo-Ken Nanbu earthquake. Canadian Journal of Civil Engineering 1996;23(3):727–56.
[6] Watanabe E, Sugiuara K, Nagata K, Kitane Y. Performances and damages to steel structures during the 1995 Hyogoken–Nanbu earthquake. Engineering Structures 1998;20(4–6):282–90.
[7] Sumner EA, Mays TW, Murray TM. Cyclic testing of bolted moment end-plate connections. Research report SAC/BD-00/21. CE/VPI-ST 00/03. Blacksburg (VA): Department of Civil and Environmental Engineering, Virginia Polytechnic Institute and State University; 2000.
[8] Egor Popov, Shakhzod Takhirov. Bolted large seismic steel beam-to-column connections part 1: experimental study. Engineering Structures 2002;24: 1523–34.
[9] Takhirov S, Popov E. Bolted large seismic steel beam-to-column connections part 2: numerical nonlinear analysis. Engineering Structures 2002;24: 1535–45.
[10] Coelho Ana M Girao, Bijlaard Frans SK, Nol Gresnigt, Simoes da Silva Luis. Experimental assessment of the behaviour of bolted T-stub connections made up of welded plates. Journal of Constructional Steel Research 2003; doi:10.1016/j.jcsr.2003.08.008.
[11] Coelho Ana M Girao, Bijlaard Frans SK, Simoes da Silva Luis. Experimental assessment of the ductility of extended end plate connections. Engineering Structures 2004;26:1185–206.
[12] Shiming Chen, Gang Du. Influence of initial imperfection on the behaviour of extended bolted end-plate connections for portal frames. Journal of Constructional Steel Research 2006; doi:10.1016/j.jcsr.2006.03.004.
[13] Elghazouli AY, Malaga-Chuquitaype C, Castro JM, Orton AH. Experimental monotonic and cyclic behaviour of blind-bolted angle connections. Engineering Structures 2009; doi:10.1016/j.engstruct.2009.05.021.
[14] Sumner EA. Unified design of extended end plate moment connections subject to cyclic loading. Ph.D. dissertation. Blackburg (VA): Virginia Polytechnic Institute and State University; 2003.
[15] ANSYS element reference. ANSYS 10.0 documentation.
[16] FEMA. Recommended seismic design criteria for new steel moment frame buildings. Report no. FEMA-350. Federal Emergency Management Agency: California Universities for Research in Earthquake Engineering; 2000.
[17] AISC . Manual of steel construction. 8th ed. Chicago: American Institute of Steel Construction; 1980.
[18] Kulak Geoffrey L, Fisher John W, Struik John HA. Guide to design criteria for bolted and revited joints. Chicago: AISC; 1987.